



Comprehensive study on Sb-doped zinc oxide films deposited on c-plane Al_2O_3 substrates

Yi Cheng¹ · Jixiang Chen¹ · Xizhen Zhang¹ · Tao Yu¹ · Kun Yang¹ · Li Che¹

Received: 29 November 2017 / Accepted: 30 April 2018 / Published online: 25 May 2018
© Springer Science+Business Media, LLC, part of Springer Nature 2018

Abstract

Undoped and Sb-doped p-type ZnO films were grown on (001) sapphire using metal organic chemical vapor deposition (MOCVD) technology. The crystal, optical, and electrical properties of the undoped and Sb-doped ZnO film were investigated by X-ray diffraction (XRD), photoluminescence, optical transmittance spectroscopy and Hall measurement system. The XRD patterns indicated both films exhibited preferred orientation along c axis and had a compressive stress. Strong near-band gap emissions of both films were observed in the room temperature photoluminescence spectra. Low temperature photoluminescence spectrum of the ZnO film was dominated by a donor-bound exciton with peak at 3.365 eV. To the Sb-doped ZnO film, donor-bound exciton was buried into the free exciton with peak at 3.371 eV, and emission intensities associated acceptor enhanced. The acceptor binding energy was calculated to be 0.19 eV. The optical bandgap of the Sb-doped ZnO film was estimated to be 3.302 eV. The Sb-doped ZnO film exhibited p-type conductivity with the resistivity of $0.6729 \Omega \text{ cm}$, mobility of $6.150 \text{ cm}^2 \text{ V}^{-1} \text{ s}^{-1}$ and carrier concentration of $1.508 \times 10^{18} \text{ cm}^{-3}$.

1 Introduction

In recent decades, significant interest has emerged in the research of doped ZnO film and application based on ZnO material. ZnO is a wide direct bandgap semiconductor with a band gap of 3.37 eV [1, 2]. The exciton binding energy of ZnO is 60 meV at 300 K, which is larger than the room temperature thermal energy (26 meV), suggesting that the electron–hole pairs are stable at room temperature [3]. These properties have made ZnO attractively apply to many kinds of optoelectronic devices, such as blue-light emitting diodes [4], short-wavelength laser diodes [5], and ultraviolet photodetectors [6]. As it is well known, elements doped in ZnO film could modify its fundamental electrical and optical properties. Until now, various elements such as In [7], Cu [8], N [9], P and As have been doped into ZnO film [10, 11]. And as it is been expected, good electrical conductivity property [12], changeable electrical conductivity type, adjustable wavelength band gap [13], and flexible luminescence property in ultraviolet emission, green emission and red emission region, have been achieved in doped ZnO film

[14]. Among the various types of dopants, Sb is a prominent luminescence activator and p-type conductivity activator in ZnO film, which is considered that the antisite Sb_{Zn} plus two zinc vacancies form a $\text{Sb}_{\text{Zn}}-2\text{V}_{\text{Zn}}$ acceptor complex and create a shallow acceptor level [15]. The $\text{Sb}_{\text{Zn}}-2\text{V}_{\text{Zn}}$ acceptor complex is confirmed to have both low formation and ionized energy. Recently, it has been proved that the Sb dopant in ZnO film not only alerts the electrical properties but also affects surface morphology and preferred orientation deposition [16]. Thus Sb dopant is a kind of surfactant to enhance the crystallization of ZnO film.

Substrate temperature, chamber gas environment, and pressure are considered to be the key factors that influence on the formation mechanism of the acceptor complex in the Sb-doped ZnO film [17–19]. Under the influence of lattice mismatch, defects and dislocations could cause internal stress that exists on interface of sapphire/ZnO and could transfer into the ZnO films [20], which modifies optical and electrical properties of the ZnO film. Low temperature photoluminescence investigations could help to understand the energy level caused by $\text{Sb}_{\text{Zn}}-2\text{V}_{\text{Zn}}$ acceptor complex. However, until now the detailed research on Sb-doped ZnO films have been reported limited. Therefore, we focus on the research of structural, electrical and optical properties of the Sb-doped ZnO film because of the potential applications of ZnO film in ultraviolet optoelectronic devices. In the

✉ Yi Cheng
chengyi@dlmu.edu.cn

¹ Department of Physics, Dalian Maritime University,
Dalian 116026, People's Republic of China

work, we employ metal organic chemical vapor deposition (MOCVD) technology to deposit ZnO and Sb-doped ZnO film on sapphire substrate, because MOCVD technology and sapphire substrate have played great role in the large semiconductor commercial markets.

2 Experimental details

Undoped and Sb-doped ZnO films were deposited on c-plane Al_2O_3 substrates using the MOCVD system designed by our research group. Dimethylzinc (DMZn), high-purity O_2 and Ar_2 gas were used as the zinc source, oxidizing agent, and carrier gas, respectively. Trimethylantimony (TMSb) was used as the metal organic source of the Sb dopant. The growth temperature of the undoped and Sb-doped ZnO film was 500°C . The flows of O_2 were set at 500 sccm. The chamber pressure was maintained 150 Pa in the deposition process. Before growth, the c-plane Al_2O_3 substrates were sequentially degreased in ultrasonic baths of acetone, ethanol and deionized water for 5 min, respectively. The calculated molar ratio of Sb/Zn of the Sb doped ZnO film was 1.00%. To make ZnO film and Sb-doped ZnO film uniformly deposit, the reaction chamber has a rotary substrate carrier heated by below resistance. In order to avoid the pre-action between metal organic sources and oxygen, the metal organic sources was pour into reaction chamber latterly in comparison with oxygen. The deposition time for the undoped and Sb-doped ZnO films was 1 h, and the thickness

of the two samples were estimated to be about $1\ \mu\text{m}$ according to previous test results.

The crystalline structure of the films were characterized by X-ray diffraction (XRD) measurement with $\text{Cu K}\alpha$ radiation with $\lambda = 0.15406\ \text{nm}$ (Shimadzu XRD-600 X-ray diffractometer). The photoluminescence (PL) spectra were made using a JY spectrometer with a thermoelectrically cooled charge coupled device detector. Excitation of samples was done using a He–Cd laser with the 325 nm wavelength and 30 mW power. The optical absorption spectra were performed using a Shimadzu UV 160 spectrometer at room temperature. The electrical properties were measured by the Bio-Rad HL 5500 system using Van de Pauw method at room temperature.

3 Results and discussion

X-ray diffraction patterns of the undoped ZnO film and Sb-doped ZnO film are shown in Fig. 1a and b, which exhibit polycrystalline with hexagonal wurtzite structure and a strong preferred orientation along the c-axis. There are no diffraction peaks associated with Sb or Sb oxide in the XRD patterns, suggesting that there is no phase separation in the Sb-doped ZnO film. In contrast to the (101) diffraction peak intensity of the ZnO film, that's of the Sb-doped ZnO film decreases, which means that the orientation behavior of the Sb-doped ZnO film is improved due to Sb dopant. As reported, proper amount of dopant Sb affects the lateral

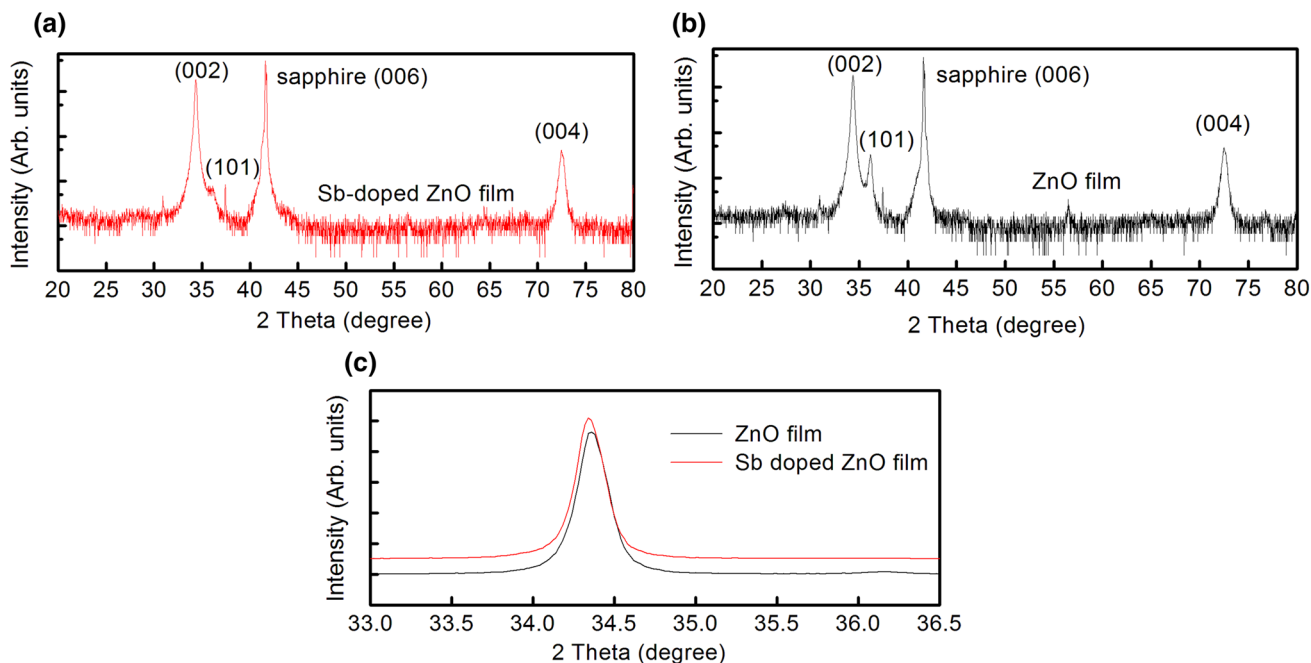


Fig. 1 XRD pattern of **a** undoped ZnO film, **b** Sb-doped ZnO film, **c** undoped ZnO film and Sb-doped ZnO film in the region of 33.0° – 36.5°

overgrowth rate and alter the facets formation, which suggests Sb acted as a surfactant to enhance the crystallization of ZnO film [16].

On basis of the XRD patterns of the undoped ZnO film and Sb-doped ZnO film, lattice constants, the stress σ , grain sizes, and full width at half peak maximum (FWHM) of the (002) diffraction peaks could be evaluated and are summarized in the Table 1. The (002) diffraction peak of the undoped ZnO film and Sb-doped ZnO film are at angle of 34.36° and 36.34° , shown in Fig. 1c. The shift of the (002) diffraction peak of Sb-doped ZnO film toward low angle implies that the lattice constant c increases after Sb doping. According to Bragg's diffraction equation,

$$2d \sin \theta = \lambda \quad (1)$$

where d is the crystalline plane distance, θ is the Bragg angle, λ is the $K\alpha_1$ wavelength and equals to 0.15406 nm. In the hexagonal wurtzite structure, the lattice constant c is equal to $2d$ for the (002) diffraction peak. Then the lattice constants c of the two samples are estimated to be 0.5218 and 0.5221 nm, respectively. Based on the lattice constants c , the stress σ in the plane of the films could be estimated using the biaxial strain model [21],

$$\sigma = -233 \times \frac{c_{\text{film}} - c_{\text{bulk}}}{c_{\text{bulk}}} \text{ (GPa)} \quad (2)$$

where c_{bulk} is lattice constant of bulk ZnO and equals to 0.5207 nm. Thus the calculated values of stress σ for pure ZnO and Sb-doped ZnO films are -0.492 and -0.626 Gpa, respectively. The negative sign of σ reveals that the residual stresses are compressive force, which caused many factors. Firstly, to sapphire and ZnO with hexagonal wurtzite structure, the lattice constant a are 4.758 and 3.249 Å, thus lattice mismatch is calculated to be 18.3% [22]. The large lattice mismatch is one of the main causes to form the dislocations and defects, which might not be constrained at the ZnO/sapphire interface and could transfer in the ZnO film. Thus, the pure ZnO film showing a compressive state is due to the dislocations at the grain boundaries. Secondly, according to stress σ values, the compressive forces in the Sb-doped ZnO film are larger than those of pure ZnO films. As reported, $\text{Sb}_{\text{Zn}}-2\text{V}_{\text{Zn}}$ complex is formed with Sb occupying the Zn site and combining with two Zn vacancies, thus the $\text{Sb}_{\text{Zn}}-2\text{V}_{\text{Zn}}$ complex easily tend to be compressed [23]. Compared with the lattice constant of bulk ZnO, lattice constants of ZnO and

Sb-doped ZnO films increase due to the compressive force. Thirdly, the difference of thermal expansion coefficient between substrate and films would produce internal force to cause compressive strain while cooling from 500°C to room temperature. Therefore, compressive force exist in ZnO and Sb-doped ZnO films and are produced by all-around factors. Based on the XRD patterns, the full width at half peak maximum (FWHM) of the (002) diffraction peaks could be calculated. According to the Scherrer equation [24],

$$D = \frac{0.9\lambda}{\beta \times \cos \theta} \quad (3)$$

where λ , θ , β are the X-ray wavelength 0.15406 nm, the diffraction angle and the FWHM of the (002) peaks. To the undoped ZnO film and Sb-doped ZnO film, the calculated average grain sizes are 39.3 and 42.0 nm, respectively.

The room temperature PL spectra in the wavelength range of 350–600 nm for both films are shown in Fig. 2. Both the undoped ZnO film and Sb-doped ZnO films shows strong near-band edge emission, peaking around 377 nm. Compared with the near-band edge emission, the luminance intensity caused by deep energy defects in green visual light region looks weak. It reveals that the rich oxygen growing condition prevents the formation of the oxygen vacancies in the undoped ZnO film and Sb-doped ZnO film because of the green emissions associated with oxygen vacancies in the ZnO lattice [25].

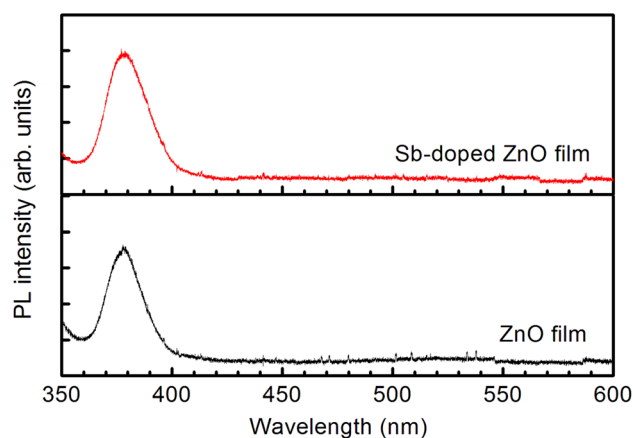


Fig. 2 PL spectra of undoped ZnO film and Sb-doped ZnO film at room temperature

Table 1 XRD parameters (position at (002) diffraction peak, FWHM, lattice constant c , stress, crystal size) of ZnO film and Sb-doped ZnO film

Sample	Position (2θ) ($^\circ$)	FWHM (β) ($^\circ$)	Lattice constant c (nm)	Stress (Gpa)	Crystal size D (nm)
ZnO	34.36	0.212	0.5218	-0.492	39.3
Sb:ZnO	34.34	0.198	0.5221	-0.626	42.0

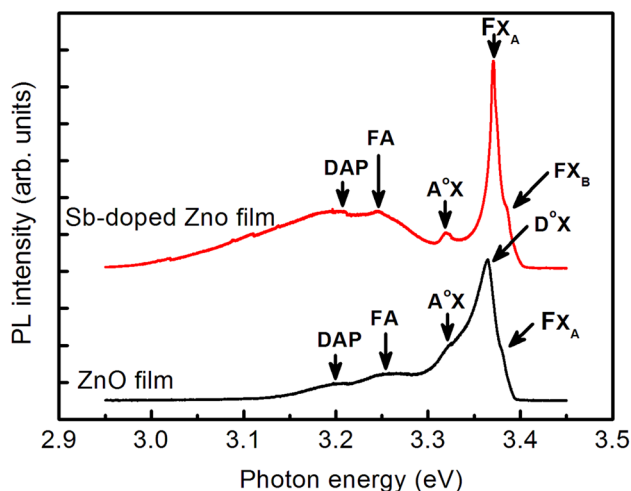


Fig. 3 Low-temperature PL spectra of undoped ZnO film and Sb-doped ZnO film at 11 K

In order to understand the shallow acceptor energy level caused by Sb dopant, we measured low temperature PL spectra for the ZnO film and the Sb-doped ZnO film with an excitation wavelength of 325 nm. Figure 3 presents the PL spectra of the undoped ZnO film and Sb-doped ZnO film at 11 K. The low temperature PL spectrum of the ZnO film shows that emission at 3.365 eV becomes dominant, which is ascribed to the donor-bound exciton (D^0X). Emissions at 3.377, 3.325, 3.258 and 3.200 eV are observed in the spectrum, which is contributed to the free exciton (FX_A), the acceptor-bound exciton (A^0X), the exciton between free electrons and acceptors (FA), and the donor–acceptor pair emission (DAP). The emission intensity of D^0X becomes dominant caused by the native defects, such as interstitial Zn [26].

In the low temperature PL spectrum of the Sb-doped ZnO film, the emission of D^0X is observed to bury into the strong free exciton with peak at 3.371 eV, expressed as FX_A . The weaker high energy shoulder appearing at 3.383 eV is the FX transition of the B-valance band, assigned as FX_B . The high intensity of the FX_A transition indicates the high recombination of the electrons from valance band to conduct band. The peak at 3.319 eV is ascribed to the A^0X emission. The peak located at 3.244 eV is considered to be the emission of FA. The emission peak at 3.200 eV is very possibly due to donor–acceptor pair, expressed as DAP emission. It is well known that the majority of p-type ZnO films doped by group-V elements have a FA emission around 3.300 eV and a DAP emission around 3.200 eV [27]. Compared with the emission intensity of pure ZnO, to the Sb-doped ZnO film, the emission of FX become dominant and the emissions associated with acceptor energy level increase greatly, such as emissions of A^0X , FA and DAP. As reported, Sb Zn donates three electrons to two adjacent V_{Zn} written as

the $Sb_{Zn}-2V_{Zn}$ complex, which become a stable acceptor state in ZnO films with low form energy and low ionized energy. The enhancement of emission intensity associated with acceptor energy level confirms the effect of the activated $Sb_{Zn}-2V_{Zn}$ complex on physical properties of ZnO films. Then the acceptor binding energy (E_A) at 11 K could be calculated using the following formula,

$$E_A = E_{gap} - E_{FA} + \frac{k_B T}{2} \quad (4)$$

where E_{FA} is the temperature-dependent transitions, and $E_{FA} = 3.244$ eV at 11 K. k_B is the Boltzmann constant, and T is the temperature. With an intrinsic band gap of $E_{gap} = 3.437$ eV, the acceptor binding energy of E_A could be calculated to be about 0.19 eV, which is similar to the theoretical calculated value of Sb-doped ZnO film [28].

To further study the optical absorption edge, optical transmittance spectra of the undoped ZnO film and Sb-doped ZnO film are measured at room temperature, shown in Fig. 4. Both films exhibit strong absorption properties in near-band gap and weak absorption in deep energy level. ZnO is a direct band gap material, for which optical band gap can be determined from absorption spectra. It obeys the relation [29],

$$ah\nu = A(h\nu - E_g)^{1/2}$$

where A is a constant, E_g is the optical bandgap, and α is the absorption coefficient. By extrapolating a plot of $(ah\nu)^2$ versus $h\nu$ to $\alpha = 0$, then the optical bandgap can be obtained. Plots of $(ah\nu)^2$ versus $h\nu$ are shown in Fig. 5. The optical bandgaps of two samples are deduced to be 3.297 and 3.302 eV, respectively. The difference of optical bandgaps might cause by compressive force exists in the undoped ZnO

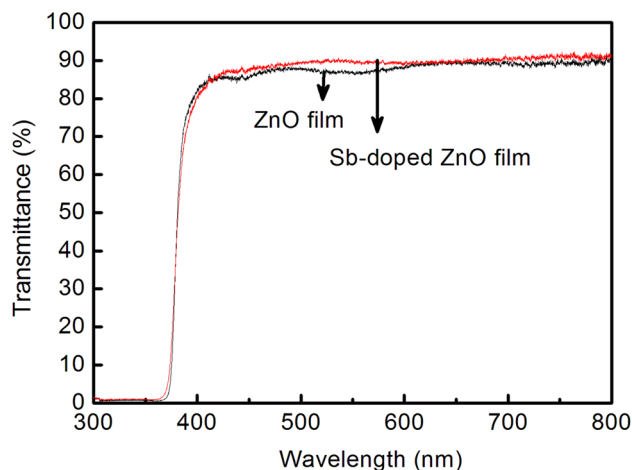


Fig. 4 Optical transmittance spectra of undoped ZnO film and Sb-doped ZnO film

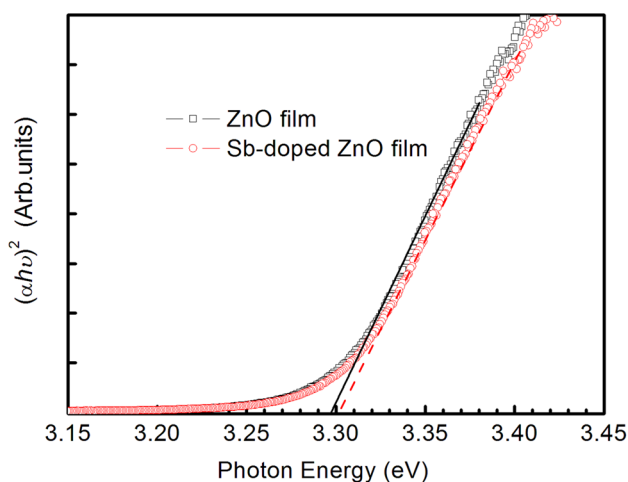


Fig. 5 Optical bandgap of undoped ZnO film and Sb-doped ZnO film

Table 2 Electrical properties of undoped ZnO film and Sb-doped ZnO films at room temperature

Sample	Conductivity type	Resistivity (Ω cm)	Mobility ($\text{cm}^2/\text{V}\cdot\text{s}$)	Carrier concentration (cm^{-3})
ZnO	n	4.226	7.520	1.965×10^{17}
Sb:ZnO	p	0.6729	6.150	1.508×10^{18}

film and Sb-doped ZnO film, or microcosmic crystal structure [30].

Using the Hall effects systems, conductivity type, resistivity, mobility and carrier concentration were characterized at room temperature, shown as Table 2. The undoped ZnO film exhibits n-type conductivity with the resistivity of 4.226 Ω cm, mobility of 7.520 $\text{cm}^2 \text{V}^{-1} \text{s}^{-1}$ and electronic concentration of $1.965 \times 10^{17} \text{cm}^{-3}$. The Sb-doped ZnO film exhibited p-type conductivity with the resistivity of 0.6729 Ω cm, mobility of 6.150 $\text{cm}^2 \text{V}^{-1} \text{s}^{-1}$ and carrier concentration of $1.508 \times 10^{18} \text{cm}^{-3}$. The undoped ZnO film exhibits n-type conductivity due to the native defects and dislocations, which make D^0X emission dominate observed in the low-temperature PL spectrum of undoped ZnO film. Compared with low temperature PL spectrum of Sb-doped ZnO, D^0X emission is covered into the FX emission, and emissions associated acceptor become strong. Thus the change in carrier type of the Sb-doped ZnO film contributes to the appearing of the new acceptor with a shallow energy level. As the above discussion, the acceptor binding energy of the the $\text{Sb}_{\text{Zn}}-2\text{V}_{\text{Zn}}$ acceptor complex is about 0.19 eV.

4 Conclusions

In summary, undoped and Sb-doped ZnO films are successfully grown on sapphire substrate under optimized growth temperature, rich oxygen flows and chamber pressure. In the low temperature PL spectrum of the Sb-doped ZnO film, FX exciton (3.371 eV), A^0X transition (3.319 eV), FA transition (3.244 eV), and DAP transition (3.200 eV) are observed, which further confirm the hall measurements about the p-type Sb-doped ZnO film with resistivity of 0.6729 Ω cm, mobility of 6.150 $\text{cm}^2 \text{V}^{-1} \text{s}^{-1}$ and carrier concentration of $1.508 \times 10^{18} \text{cm}^{-3}$. Compared with the XRD pattern of the undoped ZnO film, it is observed that Sb dopant promotes the crystallization of the film, as a consequent, crystallite sizes of the Sb-doped ZnO film increases. The optical transmittance of the Sb-doped ZnO film presents a strong absorption in the deep ultraviolet region, and optical bandgap of the Sb-doped ZnO film is estimated to be 3.302 eV.

Acknowledgements This work was supported by the National Natural Science Foundation of China (No. 21473015), the Liaoning Province Doctor Scientific Research Foundation of China (No. 201601079), the Fundamental Research Funds for the Central Universities (No. 3132017057).

References

- X.Y. Li, M.X. Chen, R.M. Yu, T.P. Zhang, D.S. Song, R.R. Liang, Q.L. Zhang, S.B. Cheng, L. Dong, A.L. Pan, Z.L. Wang, J. Zhu, C.F. Pan, Enhancing light emission of ZnO-nanofilm/Si-micro-pillar heterostructure arrays by piezo-phototronic effect. *Adv. Mater.* **27**, 4447–4453 (2015)
- A. Teke, U. Ozgur, S. Dogan, X. Gu, H. Morkoc, B. Nemeth, J. Nause, H.O. Everitt, Excitonic fine structure and recombination dynamics in single-crystalline ZnO. *Phys. Rev. B* **70**, 195207 (2004)
- M. Yilmaz, Z. Caldiran, A.R. Deniz, S. Aydogan, R. Gunturkun, A. Turut, Preparation and characterization of sol-gel-derived n-ZnO thin film for schottky diode application. *Appl. Phys. A* **119**, 547–552 (2015)
- K.W. Kim, N.J. Choi, K.B. Kim, M. Kim, S.N. Lee, Growth and characterization of nonpolar (10–10) ZnO transparent conductive oxide onsemior (11–22) GaN-based light-emitting diodes. *J. Alloys Compd.* **666**, 88–92 (2016)
- Z.K. Tang, G.K.L. Wong, P. Yu, M. Kawasaki, A. Ohtomo, H. Koinuma, Y. Segawa, Room-temperature ultraviolet laser emission from self-assembled ZnO microcrystallite thin films. *Appl. Phys. Lett.* **72**, 3270–3272 (1998)
- R. Azimirad, A. Khayatian, S. Safa, M.A. Kashi, Enhancing photoresponsivity of ultra violet photodetectors based on Fe doped ZnO/ZnOshell/core nanorods. *J. Alloys Compd.* **615**, 227–233 (2014)
- K.P. Raj, K. Sadaiyandi, A. Kennedy, S. Sagadevan, Photocatalytic and antibacterial studies of indium-doped ZnO nanoparticles synthesized by co-precipitation technique. *J. Mater. Sci. Mater. Electron.* **28**, 19025–19037 (2017)
- A. Sreedhar, H. Jung, J.H. Kwon, J. Yi, J.S. Gwag, Effect of ion beam assistance on Cu-doped ZnO thin films deposited by

- simultaneous RF and DC magnetron sputtering. *Ceram. Int.* **42**, 3064–3071 (2016)
9. A. Ievtushenko, O. Khyzhun, I. Shtepliuk, O. Bykov, R. Jakiela, S. Tkach, E. Kuzmenko, V. Baturin, O. Karpenko, O. Olifan, G. Lashkarev, X-ray photoelectron spectroscopy study of highly-doped ZnO: Al, N films grown at O-rich conditions. *J. Alloys Compd.* **722**, 683–689 (2017)
 10. P. Sharma, V. Aaryashree, S. Garg, Mukherjee, Optoelectronic properties of phosphorus doped p-type ZnO films grown by dual ion beam sputtering. *J. Appl. Phys.* **121**, 225306 (2017)
 11. E. Przewdziecka, W. Lisowski, R. Jakiela, J.W. Sobczak, A. Jablonski, M.A. Pietrzyk, A. Kozanecki, Arsenic chemical state in MBE grown epitaxial ZnO layers: doped with As, N and Sb. *J. Alloys Compd.* **687**, 937–942 (2016)
 12. M. Arshad, M.M. Ansari, A.S. Ahmed, P. Tripathi, S.S.Z. Ashraf, A.H. Naqvi, A. Azam, Band gap engineering and enhanced photoluminescence of Mg doped ZnO nanoparticles synthesized by wet chemical route. *J. Lumin.* **161**, 275–280 (2015)
 13. P. Giri, P. Chakrabarti, Effect of Mg doping in ZnO buffer layer on ZnO thin film devices for electronic applications. *Superlattices Microstruct.* **93**, 248–260 (2016)
 14. N. Tu, K.T. Nguyen, D.Q. Trung, N.T. Tuan, V.N. Do, P.T. Huy, Effects of carbon on optical properties of ZnO powder. *J. Lumin.* **174**, 6–10 (2016)
 15. S. Limpijumnong, S.B. Zhang, S.H. Wei, C.H. Park, Doping by large-size-mismatched impurities: the microscopic origin of arsenic or antimony-doped p-type zinc oxide. *Phys. Rev. Lett.* **92**, 155504 (2004)
 16. L. Zhang, H.F. Tang, J. Schieke, M. Mavrikakis, T.F. Kuech, The addition of Sb as a surfactant to GaN growth by metal organic vapor phase epitaxy. *J. Appl. Phys.* **92**, 2304–2309 (2002)
 17. C.C. Hsu, W.C. Ting, Y.T. Chen, Effects of substrate temperature on resistive switching behavior of planar ZnO resistive random access memories. *J. Alloys Compd.* **691**, 537–544 (2017)
 18. R.H. Horng, S.L. Ou, C.Y. Huang, P. Ravadgar, C.I. Wu, Effects of Ga concentration and rapid thermal annealing on the structural, optoelectronic and photoluminescence properties of Ga-doped ZnO thin films. *Thin Solid Films* **605**, 30–36 (2016)
 19. M. Hao, K. Liu, X.H. Liu, D.Y. Wang, D.H. Ba, Y.H. Xie, G.Y. Du, Y.S. Ba, Experimental investigation on photoelectric properties of ZAO thin film deposited on flexible substrate by magnetron sputtering. *Appl. Surf. Sci.* **388**, 259–267 (2016)
 20. M.M. Chen, Q.L. Zhang, L.X. Su, Y.Q. Su, J.S. Cao, Y.T.Z. Zhu, X.C. Wu, C.L. Gui, C. Yang, R. Xiang, Z.K. Tang, ZnO film with ultra-low background electron concentration grown by plasma assisted MBE using Mg film as the buffer layer. *Mater. Res. Bull.* **47**, 2673–2675 (2012)
 21. A. Osipov, S.A. Kukushkin, N.A. Feoktistov, A. Osipova, N. Venugopal, G.D. Verma, B.K. Gupta, A. Mitra, Structural and optical properties of high quality ZnO thin film on Si with SiC buffer layer. *Thin Solid Films* **520**, 6836–6840 (2012)
 22. H.H. Wu, Z.F. Hu, B. Li, H.L. Wang, Y.F. Peng, D.Z. Zhou, X.Q. Zhang, High-quality ZnO thin film grown on sapphire by hydrothermal method. *Mater. Lett.* **161**, 565–567 (2015)
 23. T. Yang, B. Yao, T.T. Zhao, G.Z. Xing, H. Wang, H.L. Pan, R. Deng, Y.R. Sui, L.L. Gao, H.Z. Wang, T. Wu, D.Z. Shen, Sb doping behavior and its effect on crystal structure, conductivity and photoluminescence of ZnO film in depositing and annealing processes. *J. Alloys Compd.* **509**, 5426–5430 (2011)
 24. Y. Cheng, K. Yang, Y. Peng, Y. Yin, J.X. Chen, B. Jing, H.W. Liang, G.T. Du, Research on the structural and optical stability of Ga₂O₃ films deposited by electron beam evaporation. *J. Mater. Sci. Mater. Electron.* **24**, 5122–5126 (2013)
 25. X.D. Meng, Y.X. Zhou, X.H. Zeng, X.B. Chen, Bright green emission and temperature dependent localized bound exciton transitions from undoped ZnO films. *Ceram. Int.* **42**, 13819–13823 (2016)
 26. F. Xiu, Z. Yang, L. Mandalapu, D. Zhao, J. Liu, W. Beyermann, High-mobility Sb-doped p-type ZnO by molecular-beam epitaxy. *Appl. Phys. Lett.* **87**, 152101 (2005)
 27. F.X. Xiu, Z. Yang, L.J. Mandalapu, J.L. Liu, Donor and acceptor competitions in phosphorus-doped ZnO. *Appl. Phys. Lett.* **88**, 152116 (2006)
 28. O. Lopatiuk-Tirpak, L. Chernyak, F. Xiu, J. Liu, S. Jang, F. Ren, S. Pearton, K. Gartsman, Y. Feldman, A. Osinsky, Studies of minority carrier diffusion length increase in p-type ZnO:Sb. *J. Appl. Phys.* **100**, 086101 (2006)
 29. H.Y. Abbasi, A. Habib, M. Tanveer, Synthesis and characterization of nanostructures of ZnO and ZnO/graphene composites for the application in hybrid solar cells. *J. Alloys Compd.* **690**, 21–26 (2017)
 30. T.P. Rao, M.C.S. Kumar, S.A. Angayarkanni, M. Ashok, Effect of stress on optical band gap of ZnO thin films with substrate temperature by spray pyrolysis. *J. Alloys Compd.* **485**, 413–417 (2009)